Inorganic Chemistry



pubs.acs.org/IC
Featured Article

# Layered Alkali Metal Titanate with the Staging Structure and Superior Electrochemical Performance

Aranee Pleng Teepakakorn, Tomohiro Tanaka, Nobuyuki Sakai, Yasuo Ebina, Takayuki Kikuchi, Renzhi Ma, Makoto Ogawa, and Takayoshi Sasaki*

Cite This: *Inorg. Chem.* 2025, 64, 16289−16296
Read Online



**ABSTRACT:** We systematically explored the formation range of $\alpha$-$NaFeO_2$-type layered titanate and its ion-exchange behaviors and electrochemical performance. The layered sodium titanate of $Na_xTi_{1-x/3}Li_{x/3}O_2$ at $x$ = 0.68−0.70 was synthesized by the solid-state reaction at 900 °C. The titanate is composed of coplanar host layers with the $\alpha$-$NaFeO_2$-type structure. The interlayer $Na^+$ ions underwent a facile exchange with other alkali metal ions in aqueous solutions at 80 °C, accompanied by concurrent exchange with proton/oxonium ions. Powder X-ray diffraction data on the products and their Rietveld refinement revealed the formation of a unique staging-structured titanate, in which the interlayer galleries are alternately occupied by incoming alkali metal ions and oxonium ions. The electrochemical intercalation−deintercalation properties for $Li^+$ and $Na^+$ ion storage were examined on the pristine sodium titanate and its ion-exchanged derivatives. The staging structure was found to provide superior electrochemical performance, which may be due to the rather open nature of the interlayer galleries, providing abundant sites for $Li^+$ and $Na^+$ ions.

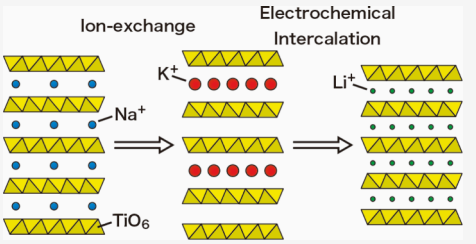


## 1. INTRODUCTION

Considerable attention has been paid to layered transition metal oxides for their useful functions, such as photocatalytic and dielectric properties.[1−7] Layered alkali metal titanates with various structures are known, as illustrated in Figure 1. A series of titanates, such as $Na_2Ti_3O_7$, $K_2Ti_4O_9$, and $Cs_2Ti_5O_{11}$, have corrugated host layers of edge-shared $TiO_6$ octahedra, which are stepped via corner-sharing every three, four, and five octahedra, respectively.[8−10] A class of lepidocrocite-type ($\gamma$-FeOOH) layered titanates with the general formula of $A_xTi_{2-y}M_yO_4$ (where A = K, Rb, Cs and M = vacancy, Li, Mg, Ni, Co, Zn, Cu, Fe(III), Mn(III))[11−14] can be regarded as their relatives with the infinite stepping width. The host layers of these compounds are negatively charged, and charge-compensating alkali metal ions are accommodated between them. The interlayer cations undergo facile ion-exchange reactions under ambient conditions.[15−18] This reactivity enables the intercalation of various organic and inorganic guest species to yield a range of nanocomposites and hybrid materials. Furthermore, the titanates can be exfoliated into colloidal individual layers via swelling, typically with some amines and organoammonium ions.[19−21] The resulting 2D oxide nanosheets can be organized as a building block into precisely designed nanostructured materials. Functionalization of the titanates through these processes has been studied extensively.[5,7,22]

There is another class of layered alkali metal titanates that are characterized by coplanar host layers based on a hexagonal linkage of $TiO_6$ octahedra (Figure 1). The titanates of the $\alpha$-$NaFeO_2$-type structure have been less investigated compared with the other compounds described above. The layered titanate based on the $\alpha$-$NaFeO_2$-type structure was first obtained by the electrochemical deintercalation of $Na^+$ from $NaTiO_2$ to form $Na_xTi^{4+}{}_{1-x}Ti^{3+}{}_xO_2$.[23,24] Isomorphous substitution of $Ti^{4+}$ in the sheet with $Co^{2+}$, $Ni^{2+}$, and $Li^+$ has been reported to yield $Na_{2/3}Co_{1/3}Ti_{2/3}O_2$, $Na_xNi_{x/2}Ti_{1-x/2}O_2$ (0.6 < $x$ < 0.66), and $Na_{0.66}Li_{0.22}Ti_{0.78}O_2$ through solid-state synthesis.[25−27] Their chemical reactivities, such as ion exchange and redox intercalation, have not been explored in depth, except for electrochemical reactivities toward possible application as a negative electrode for sodium-ion batteries.

In the present study, the $\alpha$-$NaFeO_2$-type layered alkali metal titanate of $Na_xTi_{1-x/3}Li_{x/3}O_2$ ($x \sim 0.68$) was synthesized by solid-state calcination of starting reagents $Na_2CO_3$, $Li_2CO_3$, and $TiO_2$. The ion-exchange behaviors of $Na_xTi_{1-x/3}Li_{x/3}O_2$ with the alkali metal ions ($Li^+$, $Na^+$, $K^+$, $Rb^+$, and $Cs^+$) from aqueous solutions were examined at 80 °C. We found that the ion exchange proceeded by forming a unique staging structure composed of alternately occupied and unoccupied interlayer galleries. The titanate of $Na_xTi_{1-x/3}Li_{x/3}O_2$ and its ion-

Received: April 17, 2025
Revised: July 23, 2025
Accepted: July 28, 2025
Published: August 4, 2025

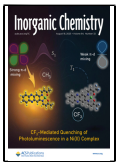







https://doi.org/10.1021/acs.inorgchem.5c01712
*Inorg. Chem.* 2025, 64, 16289−16296

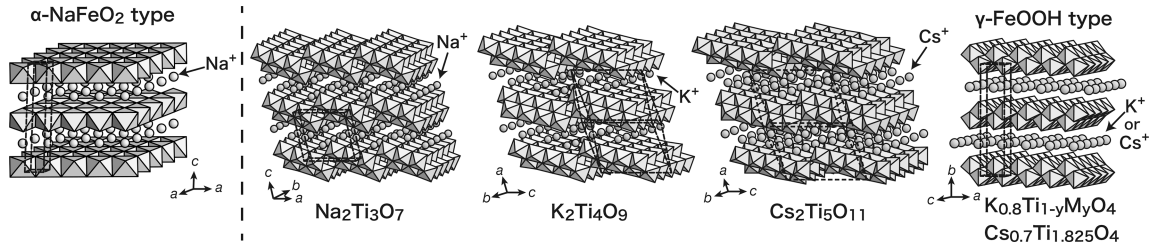


**Figure 1.** Crystal structures of various types of layered titanates. The unit cell is indicated by the broken line.

exchanged phases showed electrochemical intercalation/deintercalation properties for the storage of $Li^+$ and $Na^+$ ions.

## 2. EXPERIMENTAL SECTION

**2.1. Chemicals and Materials.** Titanium dioxide (rutile, 99.99%), lithium carbonate (99.99%), sodium carbonate (99.99%), rubidium chloride (99.9%), and cesium chloride (99.99%) were obtained from Rare Metallic, Japan, and used as received. Sodium chloride (99.5%) and potassium chloride (99.5%) were obtained from Kanto Chemical, Japan. Lithium chloride (99.0%) was purchased from Fujifilm Wako Pure Chemical, Japan. Acetylene black (HS100) was purchased from Denka, Japan. Polyvinylidene fluoride suspension (12 wt %, PVDF) was obtained from Kureha, Japan. *N*-Methyl-2-pyrrolidone (NMP, 99.5%) was purchased from Kishida Chemical, Japan. A Whatman glass fiber filter (thickness 200−300 $\mu$m) was obtained from Merck.

**2.2. Synthesis of Layered Sodium Titanate.** Reagents of $Na_2CO_3$, $Li_2CO_3$, and $TiO_2$ were intimately mixed at a molar ratio of $x/2{:}x/6{:}(1-x/3)$ for the composition $Na_xTi_{1-x/3}Li_{x/3}O_2$. The explored $x$ value was $0.60 \leq x \leq 0.80$. The mixture was placed in a Pt crucible and heated at 900 °C for 30 min for decarbonation. After cooling, the powder was ground and then heated at 900 °C for 24 h. The obtained sample, $Na_{0.68}Ti_{0.77}Li_{0.23}O_2$, referred to as NTLO, was used in the following experiments to explore its chemical reactivities.

**2.3. Ion Exchange of Layered Sodium Titanate with Alkali Metal Ions.** Ion-exchange experiments were carried out by equilibrating 0.2 g of NTLO with 20 $cm^3$ of an aqueous solution of alkali metal chloride (0.5 M) at 80 °C for 24 h. The treatment was repeated 2 times by decanting the solution with the fresh one. The products were collected by filtration, washed with deionized water several times, and then dried overnight at room temperature. The samples after the ion exchange of NTLO with alkali metal ions, $Li^+$, $Na^+$, $K^+$, $Rb^+$, and $Cs^+$, are designated as Li-NTLO, Na-NTLO, K-NTLO, Rb-NTLO, and Cs-NTLO, respectively. The ion exchange for $Li^+$ and $Na^+$ was also examined under the same conditions with K-NTLO, and the obtained samples are referred to as Li-KNTLO and Na-KNTLO, respectively.

**2.4. Electrochemical Studies.** The electrode materials (NTLO and Na-KNTLO), acetylene black, and PVDF were mixed in a weight ratio of 88:8:4 in NMP using a mixer (AR-100, Thinky). The obtained slurry was spread onto a Cu foil using blade coating and dried at 80 °C for NTLO and at 50 °C for Na-KNTLO under $N_2$ gas overnight, and it was then pressed in order to closely pack the electrode composite on the Cu foil and dried at 110 °C for NTLO and at 50 °C for Na-KNTLO under vacuum for 15 h. The lower drying temperature applied to the Na-KNTLO electrodes was intended to suppress collapse of the staging structure. The loading amount of the electrode materials was 7−12 mg/$cm^2$. The resulting electrodes were used to assemble a CR2032 coin-type cell with Li or Na foil as the counter electrode and a glass fiber filter (thickness 200−300 $\mu$m) as the separator in a dry atmosphere (<0.2 ppm of $H_2O$). $LiPF_6$ (1 M) in ethylene carbonate (EC)/diethyl carbonate (DEC) (3:7 in v/v) and 1 M sodium bis(trifluoromethanesulfonyl)imide (NaTFSI) in EC/dimethyl carbonate (DMC) (1:1 in v/v) were used as electrolytes for $Li^+$- and $Na^+$-ion batteries, respectively. The intercalation/deintercalation studies were carried out using a charge/discharge unit (HJ1001SD8, Hokuto Denko, Japan) at room temperature.

**2.5. Characterizations.** Powder X-ray diffraction (XRD) data were recorded by using a Rigaku ULTIMA IV diffractometer with monochromatic Cu K$\alpha$ radiation ($\lambda$ = 0.15405 nm). The high-resolution data for NTLO and K-NTLO were collected at BL02B1 of the SPring-8 synchrotron radiation facility (Hyogo, Japan) under the agreement from the Japan Synchrotron Radiation Research Institute (JASRI) and analyzed by Rietveld refinement with the program RIETAN-2000.[28] Scanning electron microscopy (SEM) observations were performed with JEOL, JSM-6010LA. For chemical analysis of the titanates, a weighed amount (~0.1 g) of the sample was dissolved with a mixed acid solution ($H_2SO_4$ + HF) at 135 °C for 16 h. Then, metal ion contents were determined by inductively coupled plasma-optical emission spectrometry (ICP-OES, Hitachi, SPS3520UV-DD) after appropriate dilution with water. Thermogravimetric differential thermal analysis (TG-DTA) was performed with the instrument of Rigaku, TG-8120, at a heating rate of 10 °C/min in the temperature range of 25−1000 °C.

## 3. RESULTS AND DISCUSSION

**3.1. Synthesis and Structural Characterizations.** An intimate mixture of $Na_2CO_3$, $Li_2CO_3$, and $TiO_2$ for the composition of $Na_xTi_{1-x/3}Li_{x/3}O_2$ with the $x$ value of 0.6−0.8 was heated at 900 °C. The obtained samples were composed of several tens of micrometer-sized particles with a granular to platy shape (Figure S1). Powder XRD data on the products in the range $0.68 \leq x \leq 0.70$ could be indexed in terms of the hexagonal structure with unit cell dimensions of $a \sim 0.296$ and $c \sim 1.11$ nm (Figure 2), confirming the single-phase formation of the $\alpha$-$NaFeO_2$-type layered titanate. On the other hand, impurity phases, such as $Na_2Ti_6O_{13}$ and $Li_4Ti_5O_{12}$, coexisted with the target compound outside this range.

Crystal structure of NTLO was refined on its high-resolution synchrotron XRD data based on a model with the $\alpha$-$NaFeO_2$-type layered structure (space group: $P6_3/mmc$ (No. 194)). As shown in Figure S2, the refinement led to satisfactory fitting with the residual indices $R_{wp}$ = 0.0798, $R_p$ = 0.0620, $R_I$ = 0.0392, $R_F$ = 0.027, and $s$ = 1.952. The atomic positional parameters are listed in Table S1. The results are comparable to previous reports.[27] As illustrated in Figure 1, $MO_6$ octahedra are joined via edge-sharing to form the coplanar host layer of $Ti_{0.77}Li_{0.23}O_2$. It is known that oxide layers in the $\alpha$-$NaFeO_2$-type architecture are stacked in various sequences to provide suitable coordination environments for interlayer cations.[29,30] Two of the most typical stacking modes are P2 and O3, where P and O represent the trigonal prismatic and octahedral coordination, respectively, while 2 and 3 indicate the number of oxide layers in the unit cell. The NTLO in this study adopts the P2 structure. The interlayer gallery is 0.556 nm high (= $c$/2), accommodating $Na^+$ ions at trigonal prismatic sites (2b and 2d). Their distribution in these sites was refined, revealing the preferred occupancy at the 2d site. This tendency has been reported for other isomorphous-layered metal oxides, e.g.,


https://doi.org/10.1021/acs.inorgchem.5c01712
Inorg. Chem. 2025, 64, 16289−16296

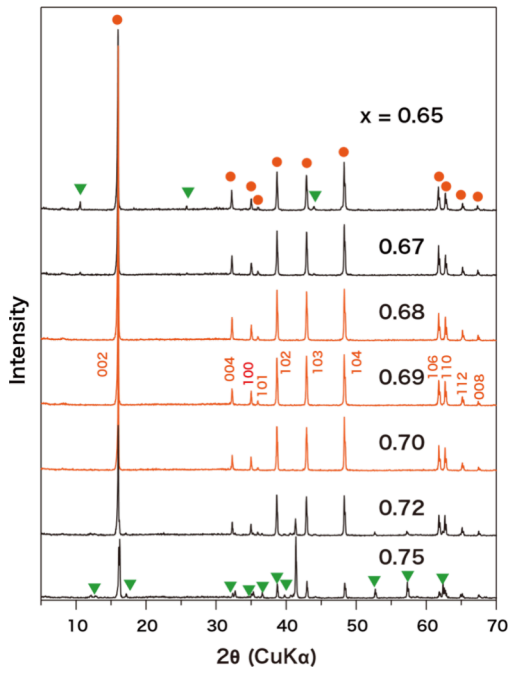


**Figure 2.** XRD patterns of calcined samples for $Na_xTi_{1-x/3}Li_{x/3}O_2$ with the $x$ value of 0.65−0.75. The peaks with orange circles are attributable to the titanate with the $\alpha$-$NaFeO_2$-type structure, while those with green triangles are from impurity phases.

$Na_{0.74}CoO_2$.[31] The interatomic distance between the metal site in the host layer and the interlayer 2b site is closer, leading to a less stable accommodation.

**3.2. Ion-Exchange Behaviors.** Ion-exchange behaviors were examined by treating NTLO with aqueous solutions of alkali metal chlorides at 80 °C. SEM observations indicate that the particle size and platelet morphology remained virtually unchanged after the treatment, suggesting a topotactic reaction process (Figure S3). The chemical composition of the samples after the ion-exchange reaction is given in Table 1. $Na^+$ ions were nearly absent when NTLO was treated with aqueous solutions of KCl, RbCl, and CsCl. It should be pointed out that the amount of incoming $K^+$, $Rb^+$, and $Cs^+$ ions is much less than that of $Na^+$ ions originally accommodated, indicating that stoichiometric ion exchange between alkali metal ions did not take place. This difference may be explained by concurrent proton exchange. Based on ignition loss results, the proton contents were estimated, as indicated in Table 1. The chemical formulas of K-NTLO, Rb-NTLO, and Cs-NTLO indicate that approximately half of the protons is accommodated in the form of oxonium ions, and another half is in the form of $H^+$. The FT-IR spectrum of ion-exchanged phases (Figure S4) is consistent with the assignment above. A broad absorption band at 3600−2700 $cm^{-1}$ and a rather sharp peak at 1600 $cm^{-1}$ are attributable to stretching and bending modes of water molecules, respectively, indicating the presence of oxonium ions. On the other hand, the strong absorption at 930 $cm^{-1}$ is characteristic of the hydroxyl group, which may be formed via bonding of a proton to the oxygen atom on the host layer. A similar feature was observed in protonated layered titanates, such as $H_2Ti_4O_9{\cdot}1.3H_2O$ and $H_2Ti_5O_{11}{\cdot}3H_2O$,[16,17,32] which contain oxonium ions and hydroxyl groups. Another noteworthy point is that the Li content remained virtually unchanged, indicating that $Li^+$ ions in the host layer were not involved in the ion-exchange reaction. Figure 3 shows

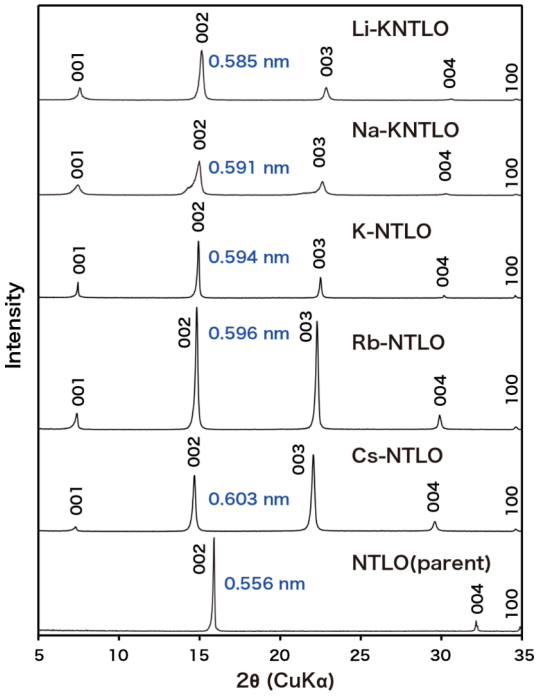


**Figure 3.** XRD patterns of NTLO and its ion-exchanged phases with alkali metal ions. Values in blue represent the $d$-spacing of the 002 peak.

powder XRD data of the ion-exchanged products. All the peaks could be indexed in terms of a hexagonal structure, and the refined unit cell parameters are summarized in Table 1. Different from the parent compound (NTLO) of $Na_{0.68}Ti_{0.77}Li_{0.23}O_2$, basal peaks having odd indices appeared, and their intensity is relatively weak compared with those with even indices. These features suggest that the layered titanate of

**Table 1. Chemical Composition and Unit Cell Dimensions of Ion-Exchanged Phases**

| sample | composition | lattice constants (nm) | |
|---|---|---|---|
| | | $a$ | $c$ |
| NTLO | $Na_{0.68}Ti_{0.77}Li_{0.23}O_2$ | 0.29611(4) | 1.1113(2) |
| Li-KNTLO[a] | $Li_{0.13}H_{0.56}Ti_{0.77}Li_{0.23}O_2{\cdot}0.39H_2O$ | 0.29879(4) | 1.1674(2) |
| Na-KNTLO | $Na_{0.17}H_{0.58}Ti_{0.77}Li_{0.17}O_2{\cdot}0.36H_2O$ | 0.29938(4) | 1.1811(2) |
| K-NTLO | $K_{0.15}H_{0.56}Ti_{0.77}Li_{0.19}O_2{\cdot}0.27H_2O$ | 0.29877(5) | 1.1818(3) |
| Rb-NTLO | $Rb_{0.13}H_{0.55}Na_{0.02}Ti_{0.77}Li_{0.21}O_2{\cdot}0.25H_2O$ | 0.29875(4) | 1.1928(2) |
| Cs-NTLO | $Cs_{0.12}H_{0.56}Na_{0.02}Ti_{0.77}Li_{0.21}\ O_2{\cdot}0.25H_2O$ | 0.29894(4) | 1.2034(3) |

[a]The Li content in the host layer is assumed to be maintained during the ion-exchange process.



https://doi.org/10.1021/acs.inorgchem.5c01712
Inorg. Chem. 2025, 64, 16289−16296

NTLO underwent some structural change upon ion exchange, as will be discussed below in depth.

On the other hand, treatment with the LiCl solution did not produce a material comparable to ion-exchanged phases with $K^+$, $Rb^+$, and $Cs^+$ ions but yielded a poorly crystalline sample, showing rather broad diffraction peaks (Figure S5a). Chemical analysis revealed that ~2/3 of $Na^+$ ions were replaced with $Li^+$ ions, and the proton exchange was not significant. The sample treated with the NaCl solution showed the XRD pattern for pristine NTLO accompanied by some minor byproducts (Figure S5b). In contrast, when K-NTLO was treated with aqueous solutions of LiCl and NaCl, an ion-exchange reaction took place in a similar way to the process of $K^+$, $Rb^+$, and $Cs^+$ ions from NTLO. Powder XRD data after the reaction show the formation of such a unique phase (Figure 3). The chemical compositions were comparable to those for K-, Rb-, and Cs-exchanged phases, except for higher degrees of hydration (Table 1).

**3.3. Staging Structure of Ion-Exchanged Materials.** As described above, after the ion-exchange process, 00*l* basal diffraction peaks ($l = 2n + 1$) appeared, suggesting a change in the stacking periodicity along the *c*-axis. There are two possibilities to account for this feature: (i) different occupancies of guests in adjacent interlayer galleries and (ii) noneven displacement of the host layers along the *c*-axis. Because no systematic extinction of diffraction peaks was recognized, five space groups, such as $P\bar{6}m2$, $P\bar{6}2m$, *P6mm*, *P622*, and *P6/mmm*, are possible. After considerations, we found that a reasonable structure model can be constructed according to the space group $P\bar{6}m2$. Then, the structure analysis was conducted for the $K^+$ ion-exchanged phase, K-NTLO, as the representative sample. The refinement yielded a reasonable convergence with the residual indices of $R_{wp}$ = 0.0597, $R_p$ = 0.0442, $R_I$ = 0.0286, $R_F$ = 0.0159, and $s$ = 1.590 (Figure 4). The structural parameters are summarized in Table 2, and the refined structure is illustrated in Figure 5. The host layers are stacked along the *c*-axis with alternate repeating spacings of 0.700 and 0.482 nm. The neighboring layers glide with respect to each other along the *a*-axis by *a*/2, generating a trigonal prismatic site for interlayer guest species. The wider interlayer galleries accommodate guest species, such as $K^+$ and $H_3O^+$ ions, while the narrower galleries are empty. The large thermal parameter may reflect from widely distributed position of these guest species, in addition to expressing their thermal vibration. As discussed above, this phase contains protons, as well as $H_3O^+$ ions. The position of protons is not available because the structure refinement is based on the XRD data.

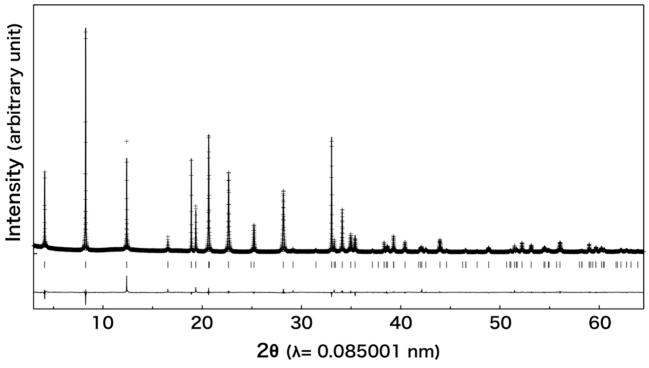


**Figure 4.** Rietveld fitting of synchrotron X-ray diffraction data for K-NTLO. Observed and calculated profiles are denoted by dotted and solid lines, respectively. The differences between them and locations of reflections are indicated at the bottom.

The $K^+$ ion-exchanged phase (K-NTLO) can be characterized by the so-called staging structure. It is well-known that graphite forms the various staging structures upon intercalation of guests, typically alkali metals.[33−36] Apart from graphite intercalation compounds, some layered compounds, such as layered double hydroxides[37−40] and interstratified clay minerals,[41−43] were reported to evolve such a unique structure. However, the formation of the staging structure in high crystallinity, which allows full structure refinement, is rare. Although there have been a number of studies for a range of layered titanates and their derivatives as described in the Section 1, to the best of our knowledge, this is the first example of the staging-structured titanate. The layer architecture of the $\alpha$-$NaFeO_2$ type is rather thin and flexible, which cannot adequately screen the electrostatic repulsion between guest cations located in neighboring interlayer space. Thus, the staging structure was produced, avoiding the occupancy of $K^+$ ions at every interlayer space. The flexible layer is also favorable, stabilizing the staging structure by forming domains similar to graphite known as the Daumas and Hérold model.[44] Recently, the staging structure was reported in the electrochemical intercalation process of $LiCoO_2$, the layer of which is also thin and flexible.[45] On the other hand, the other titanates are composed of relatively thicker corrugated layers, which can fully screen the electrostatic interaction. The interlayer cations may be considered to be isolated from those in the neighboring gallery.

The narrower interlayer spacing of 0.482 nm can be taken as the thickness of the titanate layers. This value is comparable to the layer thickness of $LiCoO_2$ with a similar layer architecture.[46] The difference of 0.218 nm (= 0.700−0.482) in the gallery heights should be related to the size of $K^+$ and $H_3O^+$ ions. It is to be noted that a change in the *c*-parameter for the ion-exchanged phases is rather modest in comparison with a variation of the ionic size for $Li^+$ to $Cs^+$ (Figure 3). This may indicate that $H_3O^+$ ions play a main role in opening the wider interlayer gallery.

**3.4. Electrochemical Intercalation/Deintercalation.** Previous study showed that NTLO can work as a superior anode material because of negligible volume change upon electrochemical cycling of the intercalation/deintercalation process.[27] Thus, it is of interest to explore the electrochemical performance of the ion-exchanged derivatives obtained in this study.

The compounds of Na-KNTLO with the staging structure and the pristine NTLO were employed as working electrodes in the coin-type cell filled with 1 M $LiPF_6$ in EC/DEC, and their electrochemical intercalation/deintercalation behaviors of $Li^+$ ions in lithium half-cells were examined at 50 mA/g in the voltage range of 0.3−3.0 V vs Li counter electrode. As shown in Figure 6, the capacity delivered in the initial $Li^+$-ion intercalation process for Na-KNTLO reached ~210 mAh/g due to the formation of a solid electrolyte interphase (SEI) and then decreased in the following cycles. The relatively large capacity observed for Na-KNTLO may be ascribed to the decomposition of water persisted in the material. After 10 cycles, the reversible capacity of 82 mAh/g was obtained, corresponding to 0.23 $Li^+$ insertion per formula unit, which is slightly smaller than the available unoccupied sites (0.25 (= 1 − 0.17 − 0.58)) in $Na_{0.17}H_{0.58}Ti_{0.77}Li_{0.17}O_2$, assuming that the


https://doi.org/10.1021/acs.inorgchem.5c01712
Inorg. Chem. 2025, 64, 16289−16296

**Table 2. Structural Parameters for K-NTLO[a]**

| atom | position | occupancy[d] | $x$ | $y$ | $z$ | $B_{eq}$ ($\times 10^{-2}$ nm$^2$) |
|---|---|---|---|---|---|---|
| G1[b] | 1b | 0.120(1) | 0 | 0 | 1/2 | 18.7(1) |
| G2[b] | 1f | 0.244 | 2/3 | 1/3 | 1/2 | 15.9 |
| M[c] | 2g | 1 | 0 | 0 | 0.20393(5) | 0.60(1) |
| O1 | 2h | 1 | 1/3 | 2/3 | 0.2864(1) | 0.98(4) |
| O2 | 2i | 1 | 2/3 | 1/3 | 0.1128(1) | 1.02(3) |

[a]Hexagonal, $P\bar{6}m2$ (No. 187), $a$ = 0.299035(1) nm, $c$ = 1.18259(1) nm. [b]$G$ = 0.15 $K^+$ + 0.27 $H_3O^+$. [c]$M$ = 0.77 $Ti^{4+}$ + 0.19 $Li^+$. [d]The occupancy factor and the atomic displacement parameter were refined independently avoiding their strong correlation. The large atomic displacement parameter may be partly due to wide positional distribution of these guest species.

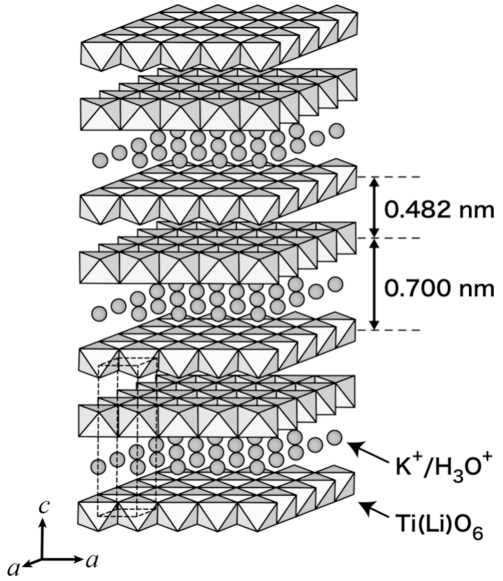


**Figure 5.** Staging structure of the $K^+$ ion-exchanged phase.

water has been decomposed. In contrast, the pristine NTLO showed a reversible capacity of 67 mAh/g, which corresponds to 0.22 $Li^+$ insertion per formula unit. This value is much smaller than the available vacancy (0.32) in $Na_{0.68}Ti_{0.77}Li_{0.23}O_2$. The crystal structure and morphology of the electrode materials that experienced the intercalation/deintercalation of $Li^+$ ions were examined. Upon 50 cycles, the 002 reflection shifted to a higher angle ($d$ = 0.492 nm) in the XRD pattern for Na-KNTLO, and the peaks due to 001 and 003 reflections disappeared (Figure 7). These changes can be ascribed to the ion exchange of $Na^+$ ions with $Li^+$ ions in their repeated intercalation/deintercalation processes because of the large excess of $Li^+$ in the system. The disappearance of 001 and 003 peaks from Na-KNTLO suggests the intercalation of $Li^+$ ions into the empty interlayer galleries during the process, leading to a loss of the staging structure. The shift of the 002 reflection was also observed for the pristine NTLO after repeated intercalation/deintercalation processes, and its $d$-spacing decreased to 0.496 nm, which is close to that of Na-KNTLO after the cycles. On the other hand, the platy morphology of Na-KNTLO and NTLO did not change significantly after 50 cycles of the process, as observed by SEM (Figure S6).

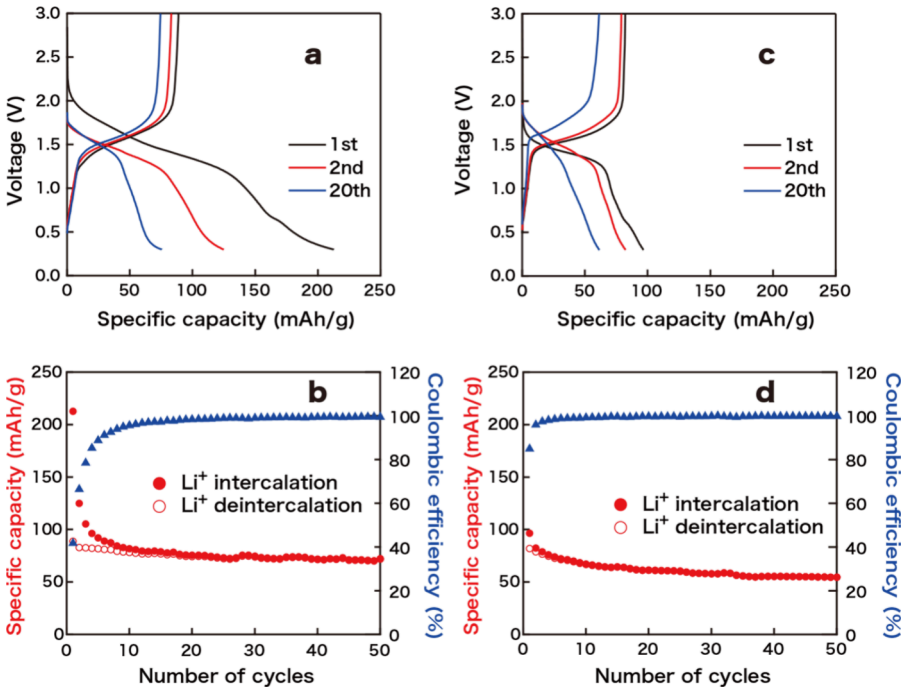


**Figure 6.** Intercalation/deintercalation curves (first, second, and 20th cycles) of $Li^+$-ion batteries using Na-KNTLO (a,b) and pristine NTLO (c,d) and their specific capacity cycle performance at 50 mA/g in the voltage range of 0.3−3.0 V, starting from the intercalation process.



https://doi.org/10.1021/acs.inorgchem.5c01712
Inorg. Chem. 2025, 64, 16289−16296

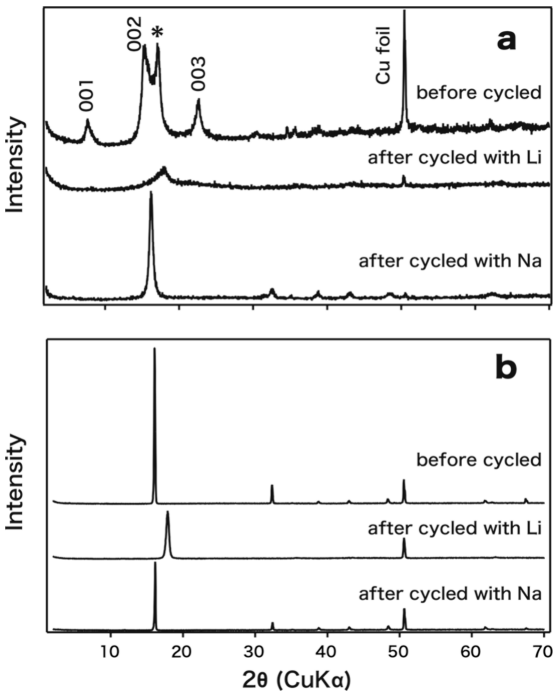


**Figure 7.** XRD patterns of Na-KNTLO (a) and pristine NTLO (b) before and after intercalation/deintercalation of $Li^+$ ions or $Na^+$ ions at 50 mA/g in the voltage range of 0.3−3.0 V. The peak designated with an asterisk ($d$ = 0.516 nm) may be ascribed to dried Na-KNTLO formed during the electrode preparation.

Intercalation/deintercalation of $Na^+$ ions was also studied for Na-KNTLO and NTLO (Figure S7). The reversible capacity obtained after 10-cycle intercalation/deintercalation was 77 mAh/g for Na-KNTLO, corresponding to 0.21 $Na^+$ insertion per formula unit, which is slightly smaller than the available vacant sites (0.25) in $Na_{0.17}H_{0.58}Ti_{0.77}Li_{0.17}O_2$. In contrast, the pristine NTLO showed a reversible capacity of 56 mAh/g, which corresponds to 0.18 $Na^+$ insertion per formula unit. This value is much smaller than the available vacancy (0.32) in $Na_{0.68}Ti_{0.77}Li_{0.23}O_2$. As shown in Figure 7, the peaks due to 001 and 003 reflections in the XRD pattern for Na-KNTLO disappeared, indicating the loss of the staging structure, as is the case in the intercalation/deintercalation of $Li^+$ ions. The 002 reflection from Na-KNTLO was shifted from $d$ = 0.577 to $d$ = 0.546 nm after the cycles, the latter of which is close to the 002 reflection from NTLO before ($d$ = 0.552 nm) and after ($d$ = 0.548 nm) intercalation/deintercalation of $Na^+$ ions. The repeated intercalation/deintercalation processes might promote the equivalent insertion of $Na^+$ ions in each gallery of Na-KNTLO, transforming its crystal structure similar to that of NTLO.

Although the staging structure of Na-KNTLO was lost during cycling, Na-KNTLO showed more efficient utilization (91% and 86%) of available vacant sites compared to the pristine NTLO (68% and 56%) in the reversible intercalation/deintercalation of $Li^+$ and $Na^+$ ions, respectively. Repeated intercalation/deintercalation into the empty interlayer spaces of the staging structure may facilitate a more efficient utilization of the interlayer galleries, resulting in a higher reversible capacity.

## 4. CONCLUSIONS

The $\alpha$-$NaFeO_2$-type layered sodium lithium titanate was synthesized by solid-state calcination for the stoichiometry of $Na_xTi_{1-x/3}Li_{x/3}O_2$ of $0.68 \leq x \leq 0.70$. $Li^+$, as well as $Ti^{4+}$ ions occupy the octahedral site in the host layer, while $Na^+$ ions are accommodated in the trigonal prismatic cavity of the interlayer space. The interlayer $Na^+$ ions could be exchanged with alkali metal ions ($Li^+$, $Na^+$, $K^+$, $Rb^+$, and $Cs^+$) and protons/oxonium ions when brought into contact with aqueous solutions of the corresponding alkali metal salts. The ion-exchange process produced the staging structure, in which the occupied and unoccupied interlayer galleries alternate. The staging-structured alkali titanates were applied as a host material for electrochemical intercalation/deintercalation of $Li^+$ and $Na^+$ ions, and we found that the specific capacities of Na-KNTLO were higher than the pristine NTLO for both $Li^+$ and $Na^+$ ions, suggesting superior performance of the staging structure for energy storage.

## ■ ASSOCIATED CONTENT

### Supporting Information

The Supporting Information is available free of charge at https://pubs.acs.org/doi/10.1021/acs.inorgchem.5c01712.

SEM images of as-synthesized NTLO, its ion-exchanged phases, and Na-KNTLO and NTLO before and after $Li^+$ ion intercalation/deintercalation; Rietveld fitting of XRD data for NTLO and its structural parameters; XRD data for NTLO treated with LiCl and NaCl; and $Na^+$-ion intercalation/deintercalation behaviors for Na-KNTLO and NTLO (PDF)

## ■ AUTHOR INFORMATION


### Corresponding Author

**Takayoshi Sasaki** − *Research Center for Materials Nanoarchitectonics (MANA), National Institute for Materials Science (NIMS), Tsukuba, Ibaraki 305-0044, Japan;* orcid.org/0000-0002-2872-0427; Email: sasaki.takayoshi@nims.go.jp

### Authors

**Aranee Pleng Teepakakorn** − *Research Center for Materials Nanoarchitectonics (MANA), National Institute for Materials Science (NIMS), Tsukuba, Ibaraki 305-0044, Japan; School of Energy Science and Engineering, Vidyasirimedhi Institute of Science and Technology (VISTEC), Rayong 21210, Thailand;* orcid.org/0000-0002-8668-3513

**Tomohiro Tanaka** − *Research Center for Materials Nanoarchitectonics (MANA), National Institute for Materials Science (NIMS), Tsukuba, Ibaraki 305-0044, Japan*

**Nobuyuki Sakai** − *Research Center for Materials Nanoarchitectonics (MANA), National Institute for Materials Science (NIMS), Tsukuba, Ibaraki 305-0044, Japan;* orcid.org/0000-0002-9395-6751

**Yasuo Ebina** − *Research Center for Materials Nanoarchitectonics (MANA), National Institute for Materials Science (NIMS), Tsukuba, Ibaraki 305-0044, Japan;* orcid.org/0000-0003-3471-9825

**Takayuki Kikuchi** − *Research Center for Materials Nanoarchitectonics (MANA), National Institute for*




https://doi.org/10.1021/acs.inorgchem.5c01712
Inorg. Chem. 2025, 64, 16289−16296

*Materials Science (NIMS), Tsukuba, Ibaraki 305-0044, Japan;* orcid.org/0000-0003-0588-2172

**Renzhi Ma** − *Research Center for Materials Nanoarchitectonics (MANA), National Institute for Materials Science (NIMS), Tsukuba, Ibaraki 305-0044, Japan;* orcid.org/0000-0001-7126-2006

**Makoto Ogawa** − *School of Energy Science and Engineering, Vidyasirimedhi Institute of Science and Technology (VISTEC), Rayong 21210, Thailand;* orcid.org/0000-0002-3781-2016

Complete contact information is available at: https://pubs.acs.org/10.1021/acs.inorgchem.5c01712

### Notes

The authors declare no competing financial interest.

## ■ ACKNOWLEDGMENTS

The authors are grateful for a Research Chair Grant 2017 (Grant number FDA-CO-2560-5655) from the National Science and Technology Development Agency (NSTDA), Thailand. This work was supported by the World Premier International Research Center Initiative (WPI), MEXT, Japan, and CREST of the Japan Science and Technology Agency (JST) (Grant No. JPMJCR22B1), Japan. The authors are grateful to Dr. Shoji Yamaguchi and Mr. Shin Kimura of the NIMS Battery Research Platform for technical assistance with the electrode preparation. We also acknowledge technical support by the Surface and Bulk Analysis Unit in NIMS for ICP-OES and XRD measurements. A.P.T. acknowledges VISTEC for the scholarship to her Ph.D. study and 1-year research exchange in MANA, NIMS, Japan.

## ■ REFERENCES

(1) Clearfield, A. Role of Ion Exchange in Solid-state Chemistry. *Chem. Rev.* **1988**, *88*, 125−148.

(2) Liu, G.; Wang, L.; Sun, C.; Yan, X.; Wang, X.; Chen, Z.; Smith, S. C.; Cheng, H. M.; Lu, G. Q. Band-to-band Visible-Light Photon Excitation and Photoactivity Induced by Homogeneous Nitrogen Doping in Layered Titanates. *Chem. Mater.* **2009**, *21*, 1266−1274.

(3) Kalantar-zadeh, K.; Ou, J. Z.; Daeneke, T.; Mitchell, A.; Sasaki, T.; Fuhrer, M. S. Two Dimensional and Layered Transition Metal Oxides. *Appl. Mater. Today.* **2016**, *5*, 73−79.

(4) He, J.; Zhang, P.; Liu, X.; Wu, S.; Hu, L.; Xu, L. Structural Characteristics and Spectral Response of Composite Transition Metal Oxide Photocatalytic Materials. *J. Mater. Sci.* **2016**, *51*, 7049−7072.

(5) Uppuluri, R.; Gupta, A. S.; Rosas, A. S.; Mallouk, T. E. Soft Chemistry of Ion-Exchangeable Layered Metal Oxides. *Chem. Soc. Rev.* **2018**, *47*, 2401−2430.

(6) Yamaguchi, T.; Oh, J.-M.; Ogawa, M. Photofunctions of Dye-Clay Hybrids: Recent Developments. In *Dyes and Photoactive Molecules in Microporous Systems*; Martínez-Martínez, V.; Arbeloa, F. L., Eds.; Springer: Cham, Switzerland, 2020; pp 251−320.

(7) Liu, T.; Miao, L.; Yao, F.; Zhang, W.; Zhao, W.; Yang, D.; Feng, Q.; Hu, D. Structure, Properties, Preparation, and Application of Layered Titanate. *Inorg. Chem.* **2024**, *63*, 1−26.

(8) Andersson, S.; Wadsley, A. D. The Crystal Structure of $Na_2Ti_3O_7$. *Acta Crystallogr.* **1961**, *14*, 1245−1249.

(9) Verbaere, A.; Tournoux, M. Contribution à l'étude des Titanates de Métaux Monovalents. Étude Structurale de $Tl_2Ti_4O_9$. *Bull. Soc. Chim. Fr.* **1973**, *4*, 1237−1241.

(10) Grey, I. E.; Madsen, I. C.; Watts, J. A.; Bursill, L. A.; Kwiatkowska, J. New Cesium Titanate Layer Structures. *J. Solid State Chem.* **1985**, *58*, 350−356.

(11) Reid, A. F.; Mumme, W. G.; Wadsley, A. D. A New Class of Compound $M_x^+A_x^{3+}Ti_{2-x}O_4$ ($0.60 < x < 0.80$) Typified by $Rb_xMn_xTi_{2-x}O_4$. *Acta Cryst. B* **1968**, *24*, 1228−1233.

(12) Hervieu, M.; Raveau, B. Structures en Feuillets Avec Sites Octaédriques Lacunaires: Les Titanates Non Stœchiométriques $Cs_{4x}Ti_{2-x}O_4$. *Rev. Chim. Miner.* **1981**, *18*, 642.

(13) Groult, D.; Mercey, C.; Raveau, B. Nouveaux oxydes à structure en feuillets: Les titanates de Potassium Non-Stoechiométriques $K_x(M_yTi_{2-y})O_4$. *J. Solid State Chem.* **1980**, *32*, 289−296.

(14) Grey, I. E.; Li, C.; Madsen, I. C.; Watts, J. A. The Stability and Structure of $Cs_x[Ti_{2-x/4}\square_{x/4}]O_4$, $0.61 < x < 0.65$. *J. Solid State Chem.* **1987**, *66*, 7−19.

(15) Izawa, H.; Kikkawa, S.; Koizumi, M. Ion Exchange and Dehydration of Layered (Sodium and Potassium) Titanates, $Na_2Ti_3O_7$ and $K_2Ti_4O_9$. *J. Phys. Chem.* **1982**, *86*, 5023−5026.

(16) Sasaki, T.; Watanabe, M.; Komatsu, Y.; Fujiki, Y. Layered Hydrous Titanium Dioxide: Potassium Ion Exchange and Structural Characterization. *Inorg. Chem.* **1985**, *24*, 2265−2271.

(17) Sasaki, T.; Watanabe, M.; Michiue, Y.; Komatsu, Y.; Izumi, F.; Takenouchi, S. Preparation and Acid-Base Properties of a Protonated Titanate with the Lepidocrocite-like Layer Structure. *Chem. Mater.* **1995**, *7*, 1001−1007.

(18) Ide, Y.; Sadakane, M.; Sano, T.; Ogawa, M. Functionalization of Layered Titanates. *J. Nanosci. Nanotechnol.* **2014**, *14*, 2135−2147.

(19) Sasaki, T.; Watanabe, M. Osmotic Swelling to Exfoliation. Exceptionally High Degrees of Hydration of a Layered Titanate. *J. Am. Chem. Soc.* **1998**, *120*, 4682−4689.

(20) Wang, L.; Sasaki, T. Titanium Oxide Nanosheets: Graphene Analogues with Versatile Functionalities. *Chem. Rev.* **2014**, *114*, 9455−9486.

(21) Song, Y.; Sakai, N.; Ebina, Y.; Iyi, N.; Kikuchi, T.; Ma, R.; Ishida, Y.; Sasaki, T. Systematic Study on Swelling/Delamination of Layered Metal Oxides with Quaternary Ammonium Ions: Production of Well-Shaped/Oversized Unilamellar Nanosheets. *Small Methods* **2025**, *9*, No. 2401055.

(22) Osada, M.; Sasaki, T. Two-Dimensional Dielectric Nanosheets: Novel Nanoelectronics from Nanocrystal Building Blocks. *Adv. Mater.* **2012**, *24*, 210−228.

(23) Maazaz, A.; Delmas, C.; Hagenmuller, P. A Study of the $Na_xTiO_2$ System by Electrochemical Deintercalation. *J. Incl. Phenom.* **1983**, *1*, 45−51.

(24) Akimoto, J.; Takei, H. Growth and Structure Analysis of Nonstoichiometric Single Crystal $Na_xTiO_2$ ($x$∼0.5) with the $\alpha$-$NaFeO_2$ Type Structure. *J. Solid State Chem.* **1990**, *85*, 31−37.

(25) Yu, H.; Ren, Y.; Xiao, D.; Guo, S.; Zhu, Y.; Qian, Y.; Gu, L.; Zhou, H. An Ultrastable Anode for Long-Life Room-Temperature Sodium-Ion Batteries. *Angew. Chem., Int. Ed.* **2014**, *53*, 8963−8969.

(26) Fielden, R.; Obrovac, M. N. Low Voltage Sodium Intercalation in $Na_xNi_{x/2}Ti_{1-x/2}O_2$ ($0.5 \leq x \leq 1.0$). *J. Electrochem. Soc.* **2014**, *161*, A1158−A1163.

(27) Wang, Y.; Yu, X.; Xu, S.; Bai, J.; Xiao, R.; Hu, Y. S.; Li, H.; Yang, X. Q.; Chen, L.; Huang, X. A Zero-Strain Layered Metal Oxide as the Negative Electrode for Long-life Sodium-ion Batteries. *Nat. Commun.* **2013**, *4*, 2365.

(28) Izumi, F.; Ikeda, T. A Rietveld-Analysis Program RIETAN-98 and its Applications to Zeolites. *Mater. Sci. Forum* **2000**, *321*−*324*, 198−205.

(29) Fouassier, C.; Delmas, C.; Hagenmuller, P. Evolution Structurale et Proprietes Physiques des Phases $A_xMO_2$ (A = Na, K; M = Cr, Mn, Co) ($x \leq 1$). *Mater. Res. Bull.* **1975**, *10*, 443−450.

(30) Takada, K.; Sakurai, H.; Takayama-Muromachi, E.; Izumi, F.; Dilanian, R. A.; Sasaki, T. A New Superconducting Phase of Sodium Cobalt Oxide. *Adv. Mater.* **2004**, *16*, 1901−1905.

(31) Berthelot, R.; Carlier, D.; Delmas, C. Electrochemical Investigation of the P2-$Na_xCoO_2$ Phase Diagram. *Nat. Mater.* **2011**, *10*, 74−80.

(32) Sasaki, T.; Komatsu, Y.; Fujiki, Y. Protonated Pentatitanate: Preparation, Characterizations, and Cation Intercalation. *Chem. Mater.* **1992**, *4*, 894−899.

(33) Solin, S. A. The Nature and Structural Properties of Graphite Intercalation Compounds. *Adv. Chem. Phys.* **1982**, *49*, 455−532.
(34) Safran, S. A. Stage Ordering in Intercalation Compounds. In *Solid State Physics*; Ehrenreich, H.; Turnbull, D., Eds.; Academic Press: Orlando, FL, 1987; Vol. *40*, pp 183−246.
(35) Xu, J.; Dou, Y.; Wei, Z.; Ma, J.; Deng, Y.; Li, Y.; Liu, H.; Dou, S. Recent Progress in Graphite Intercalation Compounds for Rechargeable Metal (Li, Na, K, Al)-Ion Batteries. *Adv. Sci.* **2017**, *4*, 1700146.
(36) Li, Y.; Lu, Y.; Adelhelm, P.; Titirici, M. M.; Hu, Y. S. Intercalation Chemistry of Graphite: Alkali Metal Ions and Beyond. *Chem. Soc. Rev.* **2019**, *48*, 4655−4687.
(37) Kooli, F.; Chisem, I. C.; Vucelic, M.; Jones, W. Synthesis and Properties of Terephthalate and Benzoate Intercalates of Mg−Al Layered Double Hydroxides Possessing Varying Layer Charge. *Chem. Mater.* **1996**, *8*, 1969−1977.
(38) Fogg, A. M.; Dunn, J. S.; O'Hare, D. Formation of Second-Stage Intermediates in Anion-Exchange Intercalation Reactions of the Layered Double Hydroxide $[LiAl_2(OH)_6]Cl{\cdot}H_2O$ As Observed by Time-Resolved, in Situ X-ray Diffraction. *Chem. Mater.* **1998**, *10*, 356−360.
(39) Iyi, N.; Kurashima, K.; Fujita, T. Orientation of an Organic Anion and Second-Staging Structure in Layered Double-Hydroxide Intercalates. *Chem. Mater.* **2002**, *14*, 583−589.
(40) Leroux, F.; Taviot-Guého, C. Fine Tuning Between Organic and Inorganic Host Structure: New Trends in Layered Double Hydroxide Hybrid Assemblies. *J. Mater. Chem.* **2005**, *15*, 3628−3642.
(41) Ijdo, W. L.; Lee, T.; Pinnavaia, T. J. Regularly Interstratified Layered Silicate Heterostructures: Precursors to Pillared Rectorite-Like Intercalates. *Adv. Mater.* **1996**, *8*, 79−83.
(42) Möller, M. W.; Hirsemann, D.; Haarmann, F.; Senker, J.; Breu, J. Facile Scalable Synthesis of Rectorites. *Chem. Mater.* **2010**, *22*, 186−196.
(43) Stöter, M.; Gödrich, S.; Feicht, P.; Rosenfeldt, S.; Thurn, H.; Neubauer, J. W.; Seuss, M.; Lindner, P.; Kalo, H.; Möller, M.; Fery, A.; Förster, S.; Papastavrou, G.; Breu, J. Controlled Exfoliation of Layered Silicate Heterostructures into Bilayers and Their Conversion into Giant Janus Platelets. *Angew. Chem., Int. Ed.* **2016**, *55*, 7398−7402.
(44) Daumas, N.; Hérold, A. Relations between Phase Concept and Reaction Mechanics in Graphite Insertion Compounds. *C. R. Seances Acad. Sci., Ser. C* **1969**, *268*, 373.
(45) Ohnishi, T.; Mitsuishi, K.; Takada, K. In Situ X-ray Diffraction of $LiCoO_2$ in Thin-Film Batteries under High-Voltage Charging. *ACS Appl. Energy Mater.* **2021**, *4*, 14372−14379.
(46) Shao-Horn, Y.; Croguennec, L.; Delmas, C.; Nelson, E. C.; O'Keefe, M. A. Atomic Resolution of Lithium Ions in $LiCoO_2$. *Nat. Mater.* **2003**, *2*, 464−467.





https://doi.org/10.1021/acs.inorgchem.5c01712
*Inorg. Chem.* 2025, 64, 16289−16296